Hydrol. Earth Syst. Sci. Discuss., 9, 12103–12143, 2012
www.hydrol-earth-syst-sci-discuss.net/9/12103/2012/
doi:10.5194/hessd-9-12103-2012

Hydrology and Earth System Sciences Discussions

Propagation of soil moisture memory to runoff and evapotranspiration

R. Orth and S. I. Seneviratne

Institute for Atmospheric and Climate Science, ETH Zurich, Universitätsstrasse 16, 8092 Zurich, Switzerland

Received: 10 October 2012 – Accepted: 20 October 2012 – Published: 26 October 2012

Correspondence to: R. Orth (rene.orth@env.ethz.ch)

Published by Copernicus Publications on behalf of the European Geosciences Union.

Abstract

As a key variable of the land-climate system soil moisture is a main driver of runoff and evapotranspiration under certain conditions. Soil moisture furthermore exhibits outstanding memory (persistence) characteristics. Also for runoff many studies report distinct low frequency variations that represent a memory. Using data from over 100 near-natural catchments located across Europe we investigate in this study the connection between soil moisture memory and the respective memory of runoff and evapotranspiration on different time scales. For this purpose we use a simple water balance model in which dependencies of runoff (normalized by precipitation) and evapotranspiration (normalized by radiation) on soil moisture are fitted using runoff observations. The model therefore allows to compute memory of soil moisture, runoff and evapotranspiration on catchment scale. We find considerable memory in soil moisture and runoff in many parts of the continent, and evapotranspiration also displays some memory on a monthly time scale in some catchments. We show that the memory of runoff and evapotranspiration jointly depend on soil moisture memory and on the strength of the coupling of runoff and evapotranspiration to soil moisture. Furthermore we find that the coupling strengths of runoff and evapotranspiration to soil moisture depend on the shape of the fitted dependencies and on the variance of the meteorological forcing. To better interpret the magnitude of the respective memories across Europe we finally provide a new perspective on hydrological memory by relating it to the mean duration required to recover from anomalies exceeding a certain threshold.

1 Introduction

Many past and recent publications have pointed out the remarkable persistence characteristics of soil moisture (Delworth and Manabe, 1988; Vinnikov and Yeserkepova, 1991; Entin et al., 2000; Koster and Suarez, 2001; Schlosser and Milly, 2002; Wu and Dickinson, 2004; Seneviratne et al., 2006a; Koster et al., 2010; Seneviratne and Koster,

HESSD
9, 12103–12143, 2012

2012). This soil moisture persistence, hereafter referred to as "memory", is caused by the integrative nature of soil moisture as water storage. It has been found in observations and models, at point scale and on continental scales. Furthermore also for other land-surface variables, persistence characteristics have been reported, even if less pronounced than for soil moisture. For instance runoff exhibits distinct low frequency variations that represent a memory resulting from a recession behavior of the runoff response following a precipitation event (Rodriguez-Iturbe and Valdes, 1979; Lins, 1997; Labat, 2008; Gudmundsson et al., 2011).

Given the important role of soil moisture in the hydrological system and for land-atmosphere interactions (e.g. Seneviratne et al., 2010, for a review), the question arises if its memory may propagate to other quantities that are at least partly driven by soil moisture. For example, runoff and evapotranspiration may be highly dependent on soil moisture under certain conditions (Eagleson, 1978; Koster and Milly, 1997; Koster et al., 2004; Botter et al., 2007; Bisselink and Dolman, 2009; Kirchner, 2009; Teuling et al., 2009), therefore soil moisture memory may induce persistence in these quantities.

This study investigates under which conditions and to which extent soil moisture memory may propagate to runoff and/or evapotranspiration. In particular for runoff, this question is of high importance in relation with water resource management. Following the approach proposed in Orth et al. (2012), we calibrate a simple hydrological model (Koster and Mahanama, 2012) with runoff measurements from 106 catchments across Europe to infer memory characteristics of soil moisture, runoff and evapotranspiration. We identify drivers and properties of the memory propagation and investigate their dependencies on regional features. Moreover we determine favorable climate and land-atmosphere regimes that promote memory propagation into the climate system. In the last part of this study we investigate how the memories in soil moisture, runoff and evapotranspiration change under dry and wet conditions, which is especially relevant in the context of the predictability of extreme events (Koster et al., 2010; Mueller and Seneviratne, 2012).

HESSD
9, 12103–12143, 2012

2 Methodology

2.1 Simple water-balance model

We use a simple water-balance model adapted from Koster and Mahanama (2012) in this study. The revised formulation used here has been introduced and discussed in Orth et al. (2012). As in that study, we run the model with a daily time step. The model is based on the following water-balance equation:

$$w_{n+1} = w_n + P_n - E_n - Q_n \quad (1)$$

where w_n, the only prognostic variable of the model, is the total soil moisture content at the beginning of time step n. Over time step n, the soil moisture content is changed by the accumulated precipitation P_n, evapotranspiration E_n, and runoff Q_n, to yield an updated soil moisture content w_{n+1} at the beginning of the following time step. Note that the employed simple model is highly conceptual, and that w_n by definition stands for all water storage on land. While we refer to this term as "soil moisture", it also is impacted by e.g. groundwater and surface water storage. These impacts are indirectly reflected in the catchment-specific calibration of the model (see Sect. 2.1.2).

To model interception, a threshold of 20 % of the long-term mean daily precipitation is applied, such that any precipitation exceeding this threshold reaches the soil (Orth et al., 2012). The intercepted water is evaporated within the same time step, thereby reducing the net radiation available at the soil. As not all daily precipitation sums reach the threshold, only about 10 % (depending on precipitation characteristics) of the total precipitation is intercepted.

2.1.1 Runoff and evapotranspiration dependencies on soil moisture

In the simple water-balance model, runoff (normalized by precipitation that reaches the soil) depends on soil moisture only. To simulate a runoff recession, precipitation of day n does not run off immediately at this time step, but is distributed over the current and

HESSD
9, 12103–12143, 2012

following 50 days, whereby the fractions that run off decrease exponentially. To capture these aspects, runoff of day n is computed using the following equation (referred to as "Q function" in the following):

$$Q_n = \sum_{i=0}^{50} \left(\frac{w_{n-i}}{c_s}\right)^{\alpha} (P_{n-i} - I_{n-i}) \left(e^{-\frac{i}{\tau}} - e^{-\frac{(i+1)}{\tau}}\right) \text{ with } \alpha \geq 1 \quad (2)$$

where soil moisture is scaled by the water holding capacity, c_s, and runoff-generating precipitation is the actual precipitation P_n reduced by the interception I_n. The runoff decay time scale τ and the soil moisture exponent α are model parameters that need to be estimated for each catchment separately (see below).

Similar to runoff, the part of evapotranspiration (ET) that is not related to interception depends on soil moisture only, after being normalized by the net radiation available at the surface. It is expressed with the following relationship (hereafter referred to as "ET function"):

$$E_n - I_n = \beta_0 \left(\frac{w_n}{c_s}\right)^{\gamma} \left(\frac{R_n}{\lambda} - I_n\right) \text{ with } \gamma \leq 1 \text{ and } \beta_0 \leq 1 \quad (3)$$

where $\frac{R_n}{\lambda}$ is the net radiation scaled with the latent heat of vaporization. The model parameter β_0 allows to capture the evaporative resistance of the soil and the vegetation, whereas the parameter γ leads to a concave shape of the ET function.

2.1.2 Parameter fitting

In total 5 model parameters ($c_s, \alpha, \tau, \beta_0, \gamma$) have to be fitted to determine the Q and ET functions of a catchment. This is done for each catchment using the same optimization approach as Orth et al. (2012), whereby the optimal set of parameters is determined as the set that yields the best fit between modeled and observed runoff among 20 estimated sets (representing local maxima in the five-dimensional parameter space).

HESSD
9, 12103–12143, 2012

This fit is evaluated during July, August and September of all available years to avoid an impact of snow, which is not included in the model. Table 1 summarizes the accuracies with which the parameters are fitted, their upper and lower limits as well as maxima and minima of the actual parameter values found for the catchments considered in this study (see Sect. 3). Note that in contrast to Orth et al. (2012), we apply here an upper limit to the runoff exponent α (15) and the water holding capacity c_s (2000 mm) to accelerate the optimization process and to prevent unreasonable fitted parameter values.

2.2 Coupling of runoff and evapotranspiration to soil moisture

As this study is investigating the propagation of memory from soil moisture to runoff and ET, it is necessary to assess the extent to which runoff and ET are driven by soil moisture, which represents the total water storage of a catchment (Sect. 2.1). For this purpose, we introduce a measure of the coupling strength between soil moisture and runoff, or soil moisture and ET, respectively. According to Eq. (2), runoff depends on soil moisture and precipitation, therefore we define the coupling strength (hereafter referred to as soil moisture-runoff coupling strength $\xi(Q_n, w_n)$) as the difference between the correlations of runoff with soil moisture and precipitation:

$$\xi(Q_n, w_n) = \rho(Q_n, w_n) - \rho\left(Q_n, P_n^*\right) \tag{4}$$

where

$$P_n^* = \sum_{i=0}^{50} \left(P_{n-i} - I_{n-i}\right) \left(e^{-\frac{i}{\tau}} - e^{-\frac{(i+1)}{\tau}}\right) \tag{5}$$

P_n^* is a cumulative weighted precipitation that reflects the joint impact of the current and previous 50 daily precipitation sums on runoff on day n with decreasing impact of precipitation after day n caused by the exponentially decreasing weight applied to each precipitation event.

HESSD
9, 12103–12143, 2012

Using Eq. (3), which shows that ET is impacted by soil moisture and net radiation, we can define a similar measure for the coupling between soil moisture and ET. This measure is defined as the difference between the correlations of ET with soil moisture and net radiation, respectively (hereafter referred to as soil moisture-ET coupling strength $\xi(E_n, w_n)$):

$$\xi(E_n, w_n) = \rho(E_n, w_n) - \rho(E_n, R_n) \tag{6}$$

Similarly to the soil moisture-runoff coupling strength, $\xi(Q_n, w_n)$, it allows us to determine and to compare the impact of soil moisture on ET.

2.3 Computation of memory

To determine the persistence of soil moisture, runoff and ET that are produced by the simple water-balance model, we calculate the respective memory as an inter-annual correlation over a particular lag (see Koster and Suarez, 2001; Seneviratne and Koster, 2012): for a given quantity, the estimates of day n from all years are correlated with the estimates of day $n + \text{lag}$ from all years. To derive representative memory estimates for half-monthly periods, we compute inter-annual correlations for this period and for the preceding and subsequent 30 days (as introduced by Orth and Seneviratne, 2012, and also applied by Orth et al., 2012). For soil moisture memory, this corresponds to the following expression:

$$\rho\left(w_n, w_{n+\text{lag}}\right) = \frac{1}{t_{\text{end}} - t_{\text{start}} + 60 - \text{lag}} \sum_{i=t_{\text{start}}-30}^{t_{\text{end}}+30-\text{lag}} \rho\left(w_i, w_{i+\text{lag}}\right) \tag{7}$$

where t_{start} and t_{end} refer to the respective start and end dates of the considered half-monthly time period. Starting 30 days prior to the beginning of the half-monthly interval and finishing 30 – lag days after the end of the half-monthly period, we obtain a number of correlations of which we take a trimmed average (not shown in Eq. (7); we avoid the

HESSD
9, 12103–12143, 2012

10 % highest and 10 % lowest values, as in Orth et al., 2012) to yield a representative memory estimate for the particular half-monthly period.

In order to study the connection between soil moisture memory and the memory of runoff and ET, respectively, we consider in the following 30-day-lag memories that are computed as described above for all quantities. To assess the impact of the investigated time scale we perform the same analysis using monthly averaged data from which we compute the respective 1-month-lag memories.

The computation of the correlations described in Sect. 2.2 is performed in a similar way as in Eq. (7). Instead of correlating estimates of a given quantity at day n from all years with the estimates of day $n + \text{lag}$ from all years, we correlate estimates of one quantity at day n from all years with estimates of the other quantity at the same day n of all years. The coupling strengths for a particular half-monthly period are then computed as the difference between the respective correlations for that period.

3 Data

In order to derive a spatially distributed evaluation of soil moisture, runoff and ET memory across Europe we apply the simple water-balance model to near-natural catchments (i.e. catchments with negligible human impact) located throughout Europe. The corresponding runoff data stem from a dataset compiled by Stahl et al. (2010), who collected data from the European water archive (http://grdc.bafg.de, checked on 16 July 2012), from national ministries and meteorological agencies, as well as from the WATCH project (http://www.eu-watch.org, checked on 16 July 2012).

The simple model uses precipitation and radiation information as an input. We use satellite-measured net radiation from the NASA/GEWEX SRB project (http://eosweb.larc.nasa.gov/PRODOCS/srb/table_srb.html, checked on 16 July 2012). The precipitation data was obtained from the E-OBS dataset (http://eca.knmi.nl, checked on 16 July 2012), which is an interpolation of rain gauge measurements on a regular

HESSD
9, 12103–12143, 2012

grid across Europe, and which was developed by the ENSEMBLES project (http://ensembles-eu.metoffice.com, checked on 16 July 2012).

Note that this study therefore uses only observed (runoff, net radiation) or observationally-based (precipitation) data. Given the different limitations in data availability of runoff, precipitation and radiation, we consider a time period of 17 yr between 1984 and 2000.

Selection of catchments

Given the large number of >400 catchments contained in the Stahl et al. (2010) dataset, we had to select a subset for two reasons: (i) the parameter fitting procedure (Sect. 2.1.2) is computationally demanding and (ii) in a few catchments the fitting procedure did not work well as seen from a low correlation between modeled and observed runoff, probably due to impacts of snow (which is not included in the model). We first selected 103 catchments, for which the runoff optimization (see Sect. 2.1.2) was at least as good as for the 13 catchments previously used in Orth et al. (2012). As only one of those 103 catchments is located in Southern Europe (Spain), we additionally selected 3 catchments in Spain to increase the spatial coverage, even if the runoff optimization displayed a slightly lower performance there (correlation between modeled and observed runoff of around 0.75, compared to ≥ 0.78 for the other catchments). This leads to the total of 106 catchments considered in this study. Corresponding information on name, coordinates, river, size, altitude and mean runoff of the considered catchments is provided in Table A1. Their locations together with their mean daily runoff are displayed in Fig. 1. The catchments are well-distributed across the continent, except for the south-east, thus allowing an analysis of persistence across a large area. As can be inferred from Table 1, the range of the fitted parameter values is larger compared to Orth et al. (2012) as we consider many more catchments, that are moreover distributed over a much wider area and across a broader range of climate regimes.

HESSD
9, 12103–12143, 2012

4 Results

In this section we first present an evaluation of the simple model's simulated runoff and its memory in the considered catchments, followed by a case study to illustrate the model behavior under different hydrological conditions. Thereafter we investigate the connection between soil moisture memory on the one hand and runoff and ET memory on the other hand, including an identification of the main driving mechanisms of these relationships. In the last part of this section we present a different view on memory as we quantify its strength in days and its variations with extreme conditions.

4.1 Evaluation of modeled runoff

The employed water-balance model was earlier validated at 13 Swiss catchments in Orth et al. (2012), with a focus on soil moisture memory. However, the present study also focuses on runoff memory and considers a much wider region that covers a large fraction of Europe. Hence, we provide a detailed evaluation of the performance of the simple water-balance model with respect to its representation of mean runoff and runoff memory at the investigated catchments. To allow an independent validation we consider monthly averages for June and October in all catchments as these months are not part of the optimization period in which the model is calibrated (see Sect. 2.1.2). The results are displayed in Fig. 2. Note that we investigate here the subset of catchments described in Sect. 3 as well as the totality of the 430 catchments of the Stahl et al. (2010) dataset in order to show a meaningful performance of the simple water balance model also in the catchments we disregard for the remainder of this study. For those catchments we run the parameter fitting procedure with one instead of 20 iterations (see Sect. 2.1.2) to reduce the computational effort (thereby increasing the risk that the resulting parameter set is only a local instead of a global maximum in the five-dimensional parameter space).

Considering all 430 catchments of the of Stahl et al. (2010) dataset, we find a rough agreement of the modeled mean daily runoff with observations in both months. The

HESSD
9, 12103–12143, 2012

numerous catchments where runoff is underestimated (especially in June) are impacted by snow melt and melting glaciers, which are both not accounted for in the model. The agreement is better when only the 106 selected catchments are considered. The fitted regression lines are closer to the identity line. The match is still slightly worse in June than in October as there are some high-altitude catchments among the selected catchments (13 % of the catchments have an average altitude higher than 1000 m above sea level (a.s.l.), see Table A1), which may therefore be impacted by snow melt. The relatively good fit between modeled and observed mean daily runoff is an interesting feature as only the *correlation* between modeled and observed runoff has been used for the calibration of the model. As shown on the right hand side of Fig. 2 the runoff memory is well captured by the model for most catchments and for the same reason discussed above the explained fraction of variance is slightly higher in October compared to June. The fitted regression lines show a minor overestimation of small runoff memories in both months. Note that the explained fraction of variance, R^2, is higher (0.70) when comparing mean monthly memories averaged from May–September (as used in Sects. 4.3 and 4.4). Interestingly, the agreement between modeled and observed runoff memory is almost the same for the totality of catchments as for the selected, reduced number of catchments, indicating that the quality of the modeled runoff memory is to some extent independent of the goodness of the runoff optimization.

4.2 Case study – Le Saulx catchment

We illustrate the model behavior and the (modeled) relationships between soil moisture, runoff and ET under dry, average and wet conditions based on a pronounced dry-down period between April and July 1998 in the Le Saulx catchment. We chose this catchment as example because it is located in Eastern France where land cover and meteorological conditions are to some extent representative for Central Europe, and also because of the especially pronounced 1998 dry-down. Figure 3 shows in the upper part the runoff function (normalized by precipitation) and ET function (normalized

HESSD
9, 12103–12143, 2012

by net radiation) fitted for that catchment based on the whole observed runoff time series. As shown by the background histogram the soil moisture content (that represents the catchment's water storage) during April through October (snow-free season) generally ranges between 25 and 100 mm, where the slopes of the normalized runoff and ET functions are similar, indicating comparable sensitivities of normalized runoff and ET with respect to soil moisture. However, under dry conditions the soil moisture content occasionally decreases to almost zero, thereby increasing the sensitivity of ET to soil moisture. Under wet conditions the soil moisture content may rise up to over 200 mm, and under such conditions the runoff is strongly dependent on soil moisture, in contrast to ET that shows a decreased sensitivity under wet conditions.

Keeping these relationships in mind, the lower part of Fig. 3 displays the evolution of modeled soil moisture, runoff and ET during the April–July 1998 dry-down period together with the corresponding precipitation and net radiation forcing. The first month, April, is rather wet (high precipitation) and cloudy (low net radiation). Consequently, the runoff is high, responds strongly to precipitation, and its evolution corresponds well with the soil moisture evolution, underlining the high sensitivity to soil moisture discussed above. In contrast to runoff, ET is lower, mostly driven by net radiation, and displays a low sensitivity to changes in soil moisture. During May and June the catchment experienced mostly sunny and dry conditions (high net radiation), only interrupted by low to medium precipitation in late May and early June. Correspondingly the soil dries out remarkably. The runoff therefore decreases to almost zero, showing almost no response to the precipitation and the following slight increase of soil moisture. This illustrates the decoupling of runoff from soil moisture under dry conditions. On the other hand, ET is comparatively high and roughly follows the strong soil moisture decrease and the subsequent stabilization, although net radiation is still the main driver as a maximum in net radiation in the second half of June causes a pronounced maximum in ET, even if soil moisture is decreasing. Finally, in July soil moisture has decreased to very low levels such that the ET level is also lower and, more importantly, despite strong day-to-day variations in net radiation, the ET evolution corresponds roughly to soil moisture.

HESSD
9, 12103–12143, 2012

4.3 Propagation of soil moisture memory

In contrast to the previous subsections that focused on particular months, all quantities discussed in this subsection (memories, correlations, coupling strengths, variances) are computed as a mean of all months between May and September. However, all mechanisms identified in the following also play a role for seasonal memory cycles of soil moisture, runoff and ET in the specific catchments.

4.3.1 Memory of soil moisture, runoff and evapotranspiration

Figure 4 displays the 30-day-lag memories of soil moisture ($\rho(w_n, w_{n+30})$), runoff ($\rho(Q_n, Q_{n+30})$) and ET ($\rho(E_n, E_{n+30})$) computed from daily data in all catchments as compared to the respective 1-month-lag memories computed from monthly averaged data. The memory patterns derived from daily and monthly data are very similar. The 1-month-lag memories are higher, which results from the aggregation of the data that minimizes the impact of day-to-day variations in the meteorological forcing.

As reported in numerous earlier studies (e.g. Delworth and Manabe, 1988; Entin et al., 2000; Robock et al., 2000; Koster and Suarez, 2001; Orth and Seneviratne, 2012) we find considerable persistence in soil moisture in almost all catchments. Largest soil moisture memory is found across Central Europe (Germany, Eastern France) and Spain. We find generally weak soil moisture memory in mountainous areas (Alps, Massif Central, Scandinavian mountains). Besides large-scale gradients there are also partly high small-scale variations (Germany, Norway). This highlights the importance of local soil and vegetation characteristics in comparison to the impact of the particular climate regime.

Interestingly, also for runoff we find medium memory in many parts of Europe, especially in the center and in the south-west, where soil moisture memory is also the highest. Apart from these rather dominant large-scale variations we find also small-scale variations, as can be seen from the partly high memory differences between nearby catchments in Central Europe, pointing out some importance of the role of local

HESSD
9, 12103–12143, 2012

catchment characteristics also for runoff memory. Figure 4 shows moreover significant memory in ET only for monthly data in some of the investigated catchments. Possible reasons for this feature will be discussed in the following subsections.

4.3.2 Controls of memory propagation

To assess the connection between soil moisture memory versus runoff and ET memory, a scatter plot of the runoff and ET memories from all catchments as a function of the corresponding soil moisture memories is presented in Fig. 5, where every point and every triangle represents one catchment. The left plot is based on daily data and shows 30-day-lag memories whereas the right plot is based on monthly data and shows 1-month-lag memories. In agreement with Fig. 4, this analysis shows that ET memories are generally lower than runoff memories. With the help of the dashed identity line we find that runoff memory is at maximum slightly larger than the corresponding soil moisture memory, which suggests that runoff memory to some extent originates from and is limited by soil moisture memory. However, in four catchments the runoff memory slightly exceeds the estimated soil moisture memory. As seen from Eq. (2) and discussed in Sect. 2.2, runoff depends on soil moisture and on the sum of weighted past daily precipitations, P_n^*, which means that memory may also propagate from the cumulative weighted precipitation to runoff. For daily data, in contrast to ordinary daily precipitation (and also to the second forcing component of the simple model, net radiation R_n), the cumulative weighted precipitation P_n^* displays some memory, with a mean value of 0.39 across all catchments for a lag of 10 days; also for a lag of 30 days a few catchments exhibit P_n^* memories of up to about 0.3 (mean of 0.07). The memory of P_n^* is strongly connected to the fitted runoff recession timescale, which makes sense as it is used in the computation of P_n^*. Even if this memory is of minor importance at long lags for most catchments, it explains why the runoff memory slightly exceeds soil moisture memory in some catchments (above-average P_n^* memory in all these catchments). At short lags (5–15 days) the memory of the cumulative weighted precipitation sum plays a more prominent role.

HESSD
9, 12103–12143, 2012

Using color coding, Fig. 5 also shows the respective soil moisture-runoff and soil moisture-ET coupling strengths (see Sect. 2.2). Runoff memories are found to be dependent on $\xi(Q_n, w_n)$. All catchments that show comparatively high runoff memories, also show comparatively high $\xi(Q_n, w_n)$ together with also relatively high soil moisture memories. This supports the above-described propagation of soil moisture memory, leading to soil moisture memory being an upper bound for runoff memory. For the ET memory the link to $\xi(E_n, w_n)$ is less clear, nonetheless most of the catchments with comparatively high ET memory also display a higher $\xi(E_n, w_n)$. In most catchments $\xi(E_n, w_n)$ is weaker than $\xi(Q_n, w_n)$, which explains why runoff memory exceeds ET memory. As can be seen especially from the analysis of monthly data, even for catchments where $\xi(Q_n, w_n)$ and $\xi(E_n, w_n)$ are similar, the runoff memories tend to be higher. This is because the memory of cumulative weighted precipitation exceeds the memory of net radiation also on a monthly time scale, which further highlights the role of the forcing memory in shaping the resulting runoff and ET memories.

Whereas runoff memories are rather similar on daily and monthly time scales because P_n^* (Eq. 5) already reflects the joint impact of many daily precipitation sums, the ET memories differ clearly. On a daily basis, ET is strongly dominated by net radiation and its variations (low $\xi(E_n, w_n)$), which consequently prevents memory propagation. On a monthly time scale, day-to-day variations of net radiation are averaged out to some extent and variations in soil moisture become more important, thereby enhancing the soil moisture-ET coupling strength. These findings highlight the importance of the time scale used in memory considerations.

When computing the memory of evaporative fraction $\frac{E_n}{R_n}$ instead of ET on a daily time scale (not shown) we find far stronger memory that is similar to soil moisture memory, underlining the strong weakening impact of daily net radiation on ET memory. Also the memory of $\frac{Q_n}{P_n}$ is similar to soil moisture memory on a daily time scale (not shown), and therefore stronger than runoff memory. This shows that also runoff memory is weakened by the atmospheric forcing (P_n^*) through its day-to-day variability.

HESSD
9, 12103–12143, 2012

Summing up, we have shown in this section that runoff and ET memory depend on (i) soil moisture memory, which acts to some extent as an upper limit, (ii) the strength of the coupling to soil moisture, and (iii) the memory of the forcing. A schematic view of these dependencies is presented in Fig. 6, with positive relationships denoted by red arrows and negative relationships shown with blue arrows. It also illustrates that the forcing memory not only supports the runoff and ET memories but also the soil moisture memory itself (Orth and Seneviratne, 2012). Moreover the scheme includes controls of $\xi(Q_n, w_n)$ and $\xi(E_n, w_n)$, which are discussed in the following subsection together with a further discussion of Fig. 6.

4.4 Soil moisture-runoff and soil moisture-ET coupling

4.4.1 Geographical distribution

Figure 7 displays the geographical distribution of the two coupling strengths estimated from Eqs. (4) and (6) and computed with daily and monthly averaged data, respectively. The geographical patterns appear to be independent of the applied time scale. As discussed in the previous section the soil moisture-runoff coupling strengths are similar for different time scales whereas the soil moisture-ET coupling strengths increase significantly in many catchments. Also the spread of the coupling strengths of all catchments increases with increasing time scale.

The soil moisture-runoff coupling $\xi(Q_n, w_n)$ is generally weak in coastal areas (Great Britain, Norway) and comparatively strong in flat, continental regions (Germany, France, Spain). However, in coastal areas around the Baltic sea (Denmark, Estonia, Finland) there is no reduction in $\xi(Q_n, w_n)$. Overall, large-scale variations are dominant, although in some regions (e.g. Norway and Great Britain) partly great differences are found for nearby catchments.

For the soil moisture-ET coupling $\xi(E_n, w_n)$ small-scale variations are more prominent than large-scale variations, especially on a monthly time scale. In Spain the strong coupling can be explained with a high correlation between soil moisture and ET due to

HESSD
9, 12103–12143, 2012

the dry regime under which soil moisture is rather low and the ET function slope rather high (see Sect. 4.2). However, the other two Spanish catchments show clearly lower $\xi(E_n, w_n)$, underlining the dominant small-scale variations of the strength of this coupling. In Norway the high $\xi(E_n, w_n)$ is due to the fact that these three catchments show the three lowest fitted β_0 (< 0.2) values and therefore a high $\xi(E_n, w_n)$, as discussed in Sect. 4.3.2.

4.4.2 Controls

Having shown that runoff and ET memory are originating from soil moisture memory and are furthermore controlled by the respective soil moisture-runoff and soil moisture-ET coupling strengths, we analyze here the two coupling strengths themselves as well as the extent to which they differ. Thereby we determine which climatic regime or catchment characteristics support or inhibit memory propagation. As shown in Fig. 6, we investigate and identify two controls for the coupling strengths: (i) the slopes of the runoff (normalized by precipitation) and ET (normalized by net radiation) functions (Eqs. 2 and 3; and shown exemplarily for the Le Saulx catchment in Fig. 3), (ii) the variance of the forcing, i.e. of cumulative weighted precipitation (P_n^*) and net radiation (R_n). We consider the forcing variances as they influence the translation of a soil moisture signal into runoff and/or ET. For instance even if the respective slope is high, the respective coupling strength may be reduced by a high forcing variance.

The catchment-specific slopes are computed as follows: For every daily soil moisture value that occurs between May and September over the whole considered time period in a particular catchment we compute the respective slopes of the normalized runoff and ET functions from their derivations with respect to soil moisture. Then we take the mean of all the slopes to derive a mean runoff function slope and a mean ET function slope for a particular catchment.

As described in Sect. 4.2 the slope is an important variable for the soil moisture-runoff or soil moisture-ET coupling strength, such that for instance a slope of zero

HESSD
9, 12103–12143, 2012

implies no impact of soil moisture whereas a high slope tends to translate changes in soil moisture into changes in runoff or ET.

Figure 8 shows the impact of both drivers described above on the two coupling strengths for daily and monthly averaged data. Every point (runoff) and every triangle (ET) represents one catchment. The respective slopes of the fitted runoff and ET functions are plotted on the y-axes and the forcing variances can be read from the color coding of the symbols.

Focusing on ET first, we find an increasing $\xi(E_n, w_n)$ with increasing mean slope of the ET function on both time scales. The large variability of coupling strengths even for similar ET function slopes is partly due to the impact of interception (reduction of the scatter when only the non-interception part of ET is considered; not shown). The radiation variances are very similar at all catchments. When comparing the variances from different time scales we find a clear reduction towards the longer, monthly time scale. This is because day-to-day variations are averaged out (see Sect. 4.3.2), which causes a stronger increase of $\xi(E_n, w_n)$ with increasing slope of the ET function and consequently higher $\xi(E_n, w_n)$.

Interestingly, $\xi(Q_n, w_n)$ does not increase with increasing runoff function slope, but instead it decreases slightly on both considered time scales. Rather than by the slope, $\xi(Q_n, w_n)$ is mainly controlled by the variance of the atmospheric forcing (cumulative weighted precipitation P_n^*). Different precipitation variances cause a clear gradient in the coupling strengths for catchments with similar slopes. The strong role of the precipitation variance for $\xi(Q_n, w_n)$ compared to the role of the radiation variance for the soil moisture-ET coupling is due to the much larger spread of the precipitation variances between all catchments. As the lowest precipitation variances coincide with low slopes we find the highest $\xi(Q_n, w_n)$ at low slopes.

The partly extreme values shown at the edge of Fig. 8, where arrows denote the direction of their true position are due to very low fitted water holding capacities and/or very low fitted β_0 values for three catchments located in Norway at the coast of the North Sea.

HESSD
9, 12103–12143, 2012

The scheme in Fig. 6 summarizes all the relationships investigated above. It also illustrates how $\xi(Q_n, w_n)$ and $\xi(E_n, w_n)$ feed back on soil moisture memory. The stronger runoff and ET respond to soil moisture, the more they tend to dampen initial soil moisture anomalies. For instance a dry anomaly causes a decrease in runoff and ET, whereas a wet soil moisture anomaly would cause a strong increase, especially in runoff (see Fig. 3). The impact of the initial soil moisture anomaly for the subsequent soil moisture memory is discussed in Sect. 4.5.

4.4.3 Differences between soil moisture-runoff and soil moisture-ET coupling

As discussed in Sect. 4.3.2, runoff memory exceeds ET memory in almost all catchments on a daily time scale and still in most catchments on a monthly time scale. This is caused by the stronger coupling of runoff to soil moisture, $\xi(Q_n, w_n)$, compared to the coupling strength of ET to soil moisture, $\xi(E_n, w_n)$, found in most catchments. The reason for this is that the runoff function slopes typically (for almost all catchments on a daily time scale and most of the catchments on a monthly time scale) exceed the ET function slopes. Also the forcing variabilities play a role. Their limiting impacts on runoff and ET memory explain why the difference between the two decreases with increasing time scale. On a daily time scale radiation variance is higher then the P_n^* variance whereas on a monthly time scale it is smaller in most catchments (see Fig. 8), which explains why ET memory increases relatively to runoff memory when moving from a daily to a monthly time scale.

The larger runoff function slopes and the consequently stronger impact of runoff on soil moisture dynamics compared to the impact of ET on soil moisture dynamics are furthermore another reason for the considerable spread of the triangles in Fig. 8. Catchments with similar ET function slopes may have very different runoff function slopes that impact soil moisture dynamics differently, thereby causing different $\xi(E_n, w_n)$.

HESSD
9, 12103–12143, 2012

4.5 Relating memory to persistence time scales

While memory is considered as lag correlation in the previous subsections and previous studies (e.g. Koster and Suarez, 2001; Orth and Seneviratne, 2012) consider memory mostly as a lag correlation, we relate the memories of soil moisture, runoff and ET here to persistence time scales. This is more easily interpretable and allows us to study the respective memories under different hydrological conditions. For the computation of this persistence time scale we proceed as follows: (i) we define "normal" conditions at a particular day as those differing at most one standard deviation (computed over the values of that day from all years) from the mean of that day over all years; (ii) we choose deviations of 1.33 and 1.66 standard deviations from the mean as thresholds for medium and strong anomalies, respectively; (iii) we select all days of the time series between May and September (focusing on the warm season we avoid cold season impacts such as snow and land cover change) that exceed a threshold and calculate for each day the delay until which the quantity of interest recovers to normal conditions; (iv) finally we take the mean of all the durations to derive a mean persistence of anomalous conditions once they have exceeded a certain threshold.

Applying this methodology to the runoff, ET and soil moisture data from all catchments we derive maps of the mean persistences of dry and wet anomalies of medium and high strength in Fig. 10. The geographical patterns of the persistences compare generally well to the mean memories derived from daily data as shown in Fig. 4, suggesting consistency between the different approaches for memory computation. Whereas soil moisture displays mean persistences over all catchments of 4–6 weeks depending on the considered anomaly, we find almost no memory for ET. Focusing therefore on soil moisture and runoff, we find that it takes generally longer to reach normal conditions for strong anomalies than for medium anomalies. In other words, the stronger an initial anomaly, the more pronounced is the following memory effect. While this is not unexpected, it has important implications for the forecasts of extreme events. Also previous studies reported an enhanced soil moisture memory following

HESSD
9, 12103–12143, 2012

hydrologically extreme conditions (Koster et al., 2010; Orth and Seneviratne, 2012). This impact of the initial soil moisture anomaly on the strength of the subsequent memory is also included in the scheme in Fig. 6.

Comparing dry and wet anomalies we find that for soil moisture dry anomalies persist longer. The reason for this may be that the climate in most European regions is generally wet which means that dry anomalies can be very large whereas wet anomalies are rather limited in their extent. Confirming this argumentation, we find stronger memory under wet conditions for the Spanish catchments. Unlike the soil moisture memory patterns, runoff memory is stronger for wet anomalies. This is because $\xi(Q_n, w_n)$ is stronger under wet conditions (see Sect. 4.2) which allows a better propagation of the soil moisture memory to runoff (see Sect. 4.3.2). Note that runoff persistences for strong, dry anomalies could not be computed for all catchments as in some catchments the threshold is only exceeded on very few days. This is because runoff values rather follow an exponential than a normal distribution.

Figure 9 displays a comparison of memories computed as lag correlation and as persistence time scales. We focus on soil moisture and runoff, as no memory was found for ET above. The reasonably high R^2 values of the linear fits indicate consistency between the two approaches, only persistence time scales computed for dry runoff anomalies correspond less well to the respective lag correlations due to the exponential distribution of the runoff values discussed above. Figure 9 also shows that dry soil moisture anomalies persist longer than respective wet anomalies whereas for runoff we find the opposite. Note that the logarithmic scale of the persistence time scales, that indicates interestingly that persistence time scales increase exponentially for a linear increase in estimated lag correlation. This underlines the red noise character of soil moisture, which was already reported by Delworth and Manabe (1988). The findings of this figure are robust even when considering persistence time scales related to other anomaly thresholds or lag correlations of other lag times.

HESSD
9, 12103–12143, 2012

5 Conclusions

Using data from over 100 catchments located across Europe we have shown that a simple water balance model is able to simulate realistic runoff as well as realistic runoff memory characteristics compared to observations, thereby expanding the validation earlier performed by Orth et al. (2012).

Further this study investigated the connection between soil moisture memory on the one hand and runoff and ET memory on the other hand. It is important to note that soil moisture in the model represents the complete terrestrial water storage, thus also including groundwater. We showed that soil moisture memory to some extent serves as an upper bound for runoff and ET memory. Furthermore we defined measures of the coupling between soil moisture and runoff as well as between soil moisture and ET and found that the strengths of these couplings also determine the memory strength of runoff and ET, respectively. These findings explain why one can infer that the memory *propagates* from soil moisture to runoff and ET as illustrated in Fig. 6. As runoff and ET are moreover driven by the meteorological forcing, also the (small) memories of cumulative weighted precipitation and net radiation play a (minor) role for the strength of their respective memories.

Comparing the results for daily and monthly time scales we find higher memory for almost the same time lag in all three quantities for monthly averaged data that is due to the reduced impact of the day-to-day variations of the meteorological forcing.

Figure 6 also displays the special role of the coupling strengths between soil moisture and runoff as well as between soil moisture and ET. We showed that the soil moisture-ET coupling is mostly controlled by the slope of the fitted (normalized) ET function whereas the soil moisture-runoff coupling is strongly related to the variance of the weighted cumulative precipitation. In most catchments the ET function slope is smaller than the runoff function slope, which is the main reason for the generally weaker coupling between soil moisture and ET and the consequently lower ET memory as compared to runoff memory.

HESSD
9, 12103–12143, 2012

In the last part of this study we introduced an alternative approach for computing memory to study its dependency on different hydrological conditions. Instead of using a lag correlation we calculated the mean time required to recover from anomalous conditions above a certain threshold to normal conditions. Applying the new methodology we found increased memory under more extreme conditions as illustrated in Fig. 6 by the positive impact of the initial soil moisture anomaly on subsequent soil moisture memory. We further point out that soil moisture memory is strongest for dry anomalies whereas runoff memory is stronger during wet anomalies. These results have important implications for sub-seasonal forecasts of dry and wet soil moisture and runoff anomalies, including drought and flood events. As the resulting persistence time scales are expressed in days, this measure of memory it is more easily interpretable, which is of particular relevance for applications and practitioners. We show consistency between the two approaches, which is furthermore underlined by the consistency of the derived geographical memory patterns for soil moisture, runoff and ET. We also find that the persistence time scales are exponentially related to the respective lag correlations, pointing out a special significance of high lag correlations identified for soil moisture.

Acknowledgements. We thank the Swiss National Foundation for financial support through the NRP61 DROUGHT-CH project. Furthermore we acknowledge the European water archive and the EU-FP6 project WATCH (http://www.eu-watch.org, checked on 28 September 2012) for sharing runoff data. We acknowledge the E-OBS dataset from the EU-FP6 project ENSEMBLES (http://ensembles-eu.metoffice.com, checked on 28 September 2012) and the data providers in the ECA&D project (http://www.ecad.eu, checked on 28 September 2012) for precipitation data as well as the NASA/GEWEX SRB project (http://eosweb.larc.nasa.gov/PRODOCS/srb/table_srb.html, checked on 28 September 2012) for sharing radiation data with us.

HESSD
9, 12103–12143, 2012

References

Bisselink, B. and Dolman, A. J.: Recycling of moisture in Europe: contribution of evaporation to variability in very wet and dry years, Hydrol. Earth Syst. Sci., 13, 1685–1697, doi:10.5194/hess-13-1685-2009, 2009. 12105

Botter, G., Porporato, A., Rodriguez-Iturbe, I., and Rinaldo, A.: Basin-scale soil moisture dynamics and the probabilistic characterization of carrier hydrologic flows: slow, leaching-prone components of the hydrologic response, Water Resour. Res., 43, W02417, doi:10.1029/2006WR005043, 2007. 12105

Delworth, T. L. and Manabe, S.: The influence of potential evaporation on the variabilities of simulated soil wetness and climate, J. Climate, 1, 523–547, 1988. 12104, 12115, 12123

Eagleson, P. S.: Climate, soil and vegetation. The expected value of annual evapotranspiration, Water Resour. Res., 14, 731–739, 1978. 12105

Entin, J. K., Robock, A., Vinnikov, K. Y., Hollinger, S. E., Liu, S., and Namkhai, A.: Temporal and spatial scales of observed soil moisture variations in the extratropics, J. Geophys. Res., 105, 11865–11877, 2000. 12104, 12115

Gudmundsson, L., Tallaksen, L. M., Stahl, K., and Fleig, A. K.: Low-frequency variability of European runoff, Hydrol. Earth Syst. Sci., 15, 2853–2869, doi:10.5194/hess-15-2853-2011, 2011. 12105

Kirchner, J.: Catchments as simple dynamical systems: catchment characterization, rainfall-runoff modeling, and doing hydrology backward, Water Resour. Res., 45, W02429, doi:10.1029/2008WR006912, 2009. 12105

Koster, R. D. and Mahanama, S.: Controls on hydroclimatic means and variability in large scale land surface models, J. Hydrometeorol., 13, 1604–1620, 2012. 12105, 12106

Koster, R. D. and Milly, P. C. D.: The interplay between transpiration and runoff formulations in land surface schemes used with atmospheric models, J. Climate, 10, 1578–1591, 1997. 12105

Koster, R. D. and Suarez, M. J.: Soil moisture memory in climate models, J. Hydrometeorol., 2, 558–570, 2001. 12104, 12109, 12115, 12122

Koster, R. D., Dirmeyer, P. A., Guo, Z., Bonan, G., Chan, E., Cox, P., Gordon, C. T., Kanae, S., Kowalczyk, E., Lawrence, D., Liu, P., Lu, C.-H., Malyshev, S., McAvaney, B., Mitchell, K., Mocko, D., Oki, T., Oleson, K., Pitman, A., Sud, Y. C., Taylor, C. M., Verseghy, D., Vasic, R.,

HESSD
9, 12103–12143, 2012

Xue, Y., and Yamada, T.: Regions of strong coupling between soil moisture and precipitation, Science, 305, 1138–1140, 2004. 12105

Koster, R. D., Mahanama, S. P. P., Yamada, T. J., Balsamo, G., Berg, A. A., Boisserie, M., Dirmeyer, P. A., Doblas-Reyes, F. J., Drewitt, G., Gordon, C. T., Guo, Z., Jeong, J.-H., Lawrence, D. M., Lee, W.-S., Li, Z., Luo, L., Malyshev, S., Merryfield, W. J., Seneviratne, S. I., Stanelle, T., van den Hurk, B. J. J. M., Vitart, F., and Wood, E. F.: Contribution of land surface initialization to subseasonal forecast skill: first results from a multi-model experiment, Geophys. Res. Lett., 37, L02402, doi:10.1029/2009GL041677, 2010. 12104, 12105, 12123

Labat, D.: Wavelet analysis of the annual discharge records of the world's largest rivers, Adv. Water Resour., 31, 109–117, 2008. 12105

Lins, H. F.: Regional streamflow regimes and hydroclimatology of the United States, Water Resour. Res., 33, 1655–1667, 1997. 12105

Mueller, B. and Seneviratne, S. I.: Hot days induced by precipitation deficits at the global scale, P. Natl. Acad. Sci. USA, 109, 12398–12403, doi:10.1073/pnas.1204330109, 2012. 12105

Orth, R. and Seneviratne, S. I.: Analysis of soil moisture memory from observations in Europe, J. Geophys. Res., 117, D15115, doi:10.1029/2011JD017366, 2012. 12109, 12115, 12118, 12122, 12123

Orth, R., Koster, R. D., and Seneviratne, S. I.: Inferring soil moisture memory from runoff observations, J. Hydrometeorol., in review, 2012. 12105, 12106, 12107, 12108, 12109, 12110, 12111, 12112, 12124

Robock, A., Vinnikov, K. Y., Srinivasan, G., Entin, J. K., Hollinger, S. E., Speranskaya, N. A., Liu, S., and Namkhai, A.: The global soil moisture data bank, B. Am. Meteorol. Soc., 81, 1281–1299, 2000. 12115

Rodriguez-Iturbe, I. and Valdes, J. B.: The geomorphologic structure of hydrologic response, Water Resour. Res., 15, 1409–1420, 1979. 12105

Schlosser, C. A. and Milly, P. C. D.: A model-based investigation of soil moisture predictability and associated climate predictability, J. Hydrometeorol., 3, 483–501, 2002. 12104

Seneviratne, S. I. and Koster, R. D.: A revised framework for analyzing soil moisture memory in climate data: derivation and interpretation, J. Hydrometeorol., 13, 404–412, 2012. 12104, 12109

Seneviratne, S. I., Koster, R. D., Gao, Z., Dirmeyer, P. A., Kowalczyk, E., Lawrence, D., Liu, P., Lu, C.-H., Oleson, D. M. K. W., and Verseghy, D.: Soil moisture memory in AGCM simulations:

HESSD
9, 12103–12143, 2012

analysis of Global Land-Atmosphere Coupling Experiment (GLACE) data, J. Hydrometeorol., 7, 1090–1112, 2006. 12104

Seneviratne, S. I., Corti, T., Davin, E. L., Hirschi, M., Jaeger, E. B., Lehner, I., Orlowsky, B., and Teuling, A. J.: Investigating soil moisture-climate interactions in a changing climate: a review, Earth-Sci. Rev., 99, 125–161, 2010. 12105

Stahl, K., Hisdal, H., Hannaford, J., Tallaksen, L. M., van Lanen, H. A. J., Sauquet, E., Demuth, S., Fendekova, M., and Jódar, J.: Streamflow trends in Europe: evidence from a dataset of near-natural catchments, Hydrol. Earth Syst. Sci., 14, 2367–2382, doi:10.5194/hess-14-2367-2010, 2010. 12110, 12111, 12112

Teuling, A., Hirschi, M., Ohmura, A., Wild, M., Reichstein, M., Ciais, P., Buchmann, N., Ammann, C., Montagnani, L., Richardson, A., Wohlfahrt, G., and Seneviratne, S.: A regional perspective on trends in continental evaporation, Geophys. Res. Lett., 36, L02404, doi:10.1029/2008GL036584, 2009. 12105

Vinnikov, K. Y. and Yeserkepova, I. B.: Soil moisture: empirical data and model results, J. Climate, 4, 66–79, 1991. 12104

Wu, W. and Dickinson, R. E.: Time scales of layered soil moisture memory in the context of land-atmosphere interaction, J. Climate, 17, 2752–2764, 2004. 12104

HESSD

9, 12103–12143, 2012

Table 1. Overview of model parameter accuracies, boundaries and the range of their respective estimates.

Parameter	Accuracy	Lower limit	Upper limit	Minimum value found	Maximum value found
Water holding capacity c_s (mm)	30	30	2000	50	2000
Inverse runoff recession timescale $\frac{1}{\tau}$ ($1\,\text{days}^{-1}$)	0.02	0.02	–	0.04	0.54
Runoff exponent α	0.2	1	15	1	15
ET exponent γ	0.03	0.03	0.99	0.03	0.99
Max ET ratio β_0	0.03	0.03	0.99	0.03	0.99

HESSD
9, 12103–12143, 2012

Table A1. Overview of catchments.

Catchment (river)	Country	Gauging station	Size (km^2)	Mean altitude (m a.s.l.)	Mean daily runoff (mm)	Catchment centroid
Grosse Mühl	Austria	Teufelmühle	455	748	1.56	48.5° N 14.0° E
Saalach	Austria	Viehhofen	158	1534	2.96	47.4° N 12.7° E
Schwarza	Austria	Gloggnitz (Adlerbrücke)	467	976	1.53	47.7° N 15.9° E
Grønå	Denmark	Rørkær	588	27	1.10	54.9° N 8.9° E
Ribe å	Denmark	Stavnanger	664	40	1.24	55.3° N 9.2° E
Skjern å	Denmark	Alergård	1061	60	1.29	56.0° N 9.1° E
Spang å	Denmark	Bredstrup	64	47	0.94	55.6° N 9.6° E
Suså	Denmark	Holløse mølle	780	40	0.69	55.4° N 11.7° E
Valgejõgi	Estonia	Vanaküla	255	102	0.79	59.5° N 25.8° E
Vihterpalu	Estonia	Vihterpalu	470	29	0.86	59.3° N 23.9° E
Kiiminginjoki	Finland	Haukipudas	3915	126	1.00	65.2° N 25.4° E
Vantaa	Finland	Oulunkylä	1895	78	0.87	60.2° N 25.0° E
L' Aisne	France	Mouron	2239	208	0.95	49.3° N 4.8° E
Le Bes	France	St-Juery	298	1200	2.28	44.8° N 3.1° E
La Bromme	France	Brommat (Edf)	109	985	2.70	44.8° N 2.7° E
Le Madon	France	Pulligny	940	329	0.99	48.5° N 6.1° E
La Maronne	France	Pleaux (Enchanet)	456	774	2.38	45.1° N 2.2° E
La Moselle	France	St-Nabord (Noir Gueux)	633	720	3.35	48.1° N 6.6° E
La Santoire	France	Condat (Roche-Pointue)	171	1148	2.13	45.3° N 2.8° E
Le Saulx	France	Vitry-En-Perthois	2109	264	1.12	48.7° N 4.6° E
La Seine	France	Bar-Sur-Seine	2344	320	0.94	48.1° N 4.4° E
La Sumene	France	Bassignac (Pont De Vendes)	413	817	1.52	45.3° N 2.4° E
La Truyere	France	Malzieu-Ville (Le Soulier)	582	1122	1.13	44.8° N 3.3° E
La Truyere	France	Neuveglise (Grandval)	1803	1069	1.17	44.9° N 3.1° E

HESSD
9, 12103–12143, 2012

Table A1. Continued.

Catchment (river)	Country	Gauging station	Size (km^2)	Mean altitude (m a.s.l.)	Mean daily runoff (mm)	Catchment centroid
Aar	Germany	Michelbach	146	395	0.68	50.2° N 8.1° E
Ammer	Germany	Weilheim	600	889	2.12	47.8° N 11.1° E
Brugga	Germany	Oberried-Ibrech	40	989	3.41	47.9° N 8.0° E
Dhron	Germany	Papiermühle	170	489	0.95	49.8° N 6.9° E
Elsava	Germany	Rück	145	356	0.72	49.8° N 9.2° E
Eder	Germany	Auhammer	489	546	1.94	50.6° N 9.6° E
Eger	Germany	Trochtelfingen	129	515	0.93	48.8° N 10.4° E
Elta	Germany	Tuttlingen	86	780	0.86	48.2° N 10.0° E
Fulda	Germany	Kämmerzell	559	432	1.03	50.6° N 9.6° E
Hasel	Germany	Wehr-Hasel	32	576	1.90	48.3° N 8.1° E
Isar	Germany	Mittenwald Karwendel	402	1625	2.66	47.5° N 11.3° E
Kinzig	Germany	Schwaibach	964	600	2.16	48.4° N 8.0° E
Lahn	Germany	Biedenkopf	309	477	1.60	50.9° N 8.5° E
Loisach	Germany	Garmisch U.D. Partnach	395	1377	2.40	47.5° N 11.1° E
Lohr	Germany	Partenstein	217	400	1.20	50.0° N 9.5° E
Mitternacher Oh	Germany	Eberhardsreuth	114	663	1.55	48.8° N 13.4° E
Murg	Germany	Rotenfels	470	662	2.93	48.8° N 8.3° E
Nims	Germany	Alsdorf-Oberecken	265	415	0.97	49.9° N 6.5° E
Oste	Germany	Rockstedt	638	31	0.86	53.3° N 9.2° E
Osterbach	Germany	Röhrnbach	121	645	1.88	49.0° N 13.2° E
Saalach	Germany	Unterjettenberg Rech	760	1211	3.34	47.7° N 12.8° E
Saale	Germany	Mehle	147	196	0.85	52.1° N 9.7° E
Sausswasser	Germany	Linden	91	894	2.14	48.7° N 13.5° E
Sieber	Germany	Hattorf	141	461	1.58	51.7° N 10.3° E
Sinn	Germany	Mittelsinn	461	456	1.19	50.2° N 9.6° E
Speller Aa	Germany	Hesselte	389	65	0.83	52.4° N 7.4° E
Tiroler Achen	Germany	Staudach	955	1139	3.15	47.8° N 12.5° E
Wertach	Germany	Biessenhofen	442	882	2.44	47.8° N 10.7° E
Wetter	Germany	Buchenbruecken	508	245	0.49	50.5° N 9.1° E
Wipper	Germany	Hachelbich	522	324	0.56	51.3° N 10.4° E
Wumme	Germany	Hellwege Schl. V	987	43	0.87	53.1° N 9.2° E
Wutach	Germany	Oberlauchringen	624	789	1.23	47.6° N 8.3° E
Zorge	Germany	Nordhausen	317	400	1.03	51.5° N 10.8° E

HESSD
9, 12103–12143, 2012

Table A1. Continued.

Catchment (river)	Country	Gauging station	Size (km^2)	Mean altitude (m a.s.l.)	Mean daily runoff (mm)	Catchment centroid
Engesetelev	Norway	Engsetvatn ndf	41	206	4.92	62.5° N 6.6° E
Etna	Norway	Etna	565	925	1.44	61.0° N 9.6° E
Etneelv	Norway	Stordalsvatn	140	611	9.09	59.7° N 6.0° E
Flisa	Norway	Knappom	1655	414	1.38	60.6° N 12.0° E
Forra	Norway	Høggås bru	458	525	3.77	63.5° N 11.4° E
Gaula	Norway	Eggafoss	663	831	2.41	63.1° N 10.3° E
Glomma	Norway	Atnasjø	468	1140	1.85	61.9° N 10.2° E
Guddalselva	Norway	Nautsundvatn	214	436	7.17	61.3° N 5.4° E
Håelv	Norway	Haugland	149	167	4.15	58.7° N 5.6° E
Jondalselv	Norway	Jondal	129	569	1.73	59.7° N 9.6° E
Jøra	Norway	Aulestad	872	812	1.51	61.2° N 10.3° E
Kløvtveitelv	Norway	Kløvtveitvatn	5	466	11.06	61.0° N 5.3° E
Lygna	Norway	Tingvatn	265	564	5.80	58.4° N 7.2° E
Moelv	Norway	Salsvatn	435	285	5.18	64.7° N 11.5° E
Nordelva	Norway	Krinsvatn	210	435	5.42	63.8° N 10.2° E
Ogna	Norway	Helleland	75	336	6.79	58.5° N 6.2° E
Øren	Norway	Øren	151	264	4.05	62.8° N 7.7° E
Oselv	Norway	Røykenes	55	328	8.63	60.3° N 5.4° E
Strandå	Norway	Strandå	27	212	5.89	67.5° N 14.9° E
Tovdalselv	Norway	Austenå	310	752	3.01	58.8° N 8.1° E
Vrangselva	Norway	Magnor	368	255	1.41	60.0° N 12.2° E
No name	Norway	Karpelv	129	194	1.72	69.7° N 30.4° E
Biely Vah	Slovakia	Vychodna	120	1055	1.21	49.1° N 19.9° E
Rajcianka	Slovakia	Poluvsie	243	706	1.18	49.1° N 18.7° E
Cabrera	Spain	Puente De Domingo Florez	559	1269	1.61	42.4° N 6.8° W
Cidacos	Spain	Yanguas	228	1335	0.45	42.1° N 2.3° W
Duero	Spain	Molinos De Duero	138	1425	1.62	41.9° N 2.8° W
Tiron	Spain	Cuzcurrita	700	944	0.45	42.5° N 3.0° W

HESSD
9, 12103–12143, 2012

Table A1. Continued.

Catchment (river)	Country	Gauging station	Size (km^2)	Mean altitude (m a.s.l.)	Mean daily runoff (mm)	Catchment centroid
Dalelven	Sweden	Ersbo	1134	728	3.45	61.3° N 13.0° E
Moelven	Sweden	Anundsjön	1457	283	1.10	63.4° N 18.3° E
Råneå	Sweden	Niemisel	3756	283	0.97	66.0° N 22.0° E
Cassarate	Switzerland	Lugano	76	970	2.90	46.0° N 9.0° E
Allan Water	United Kingdom	Kinbuck	172	245	3.07	56.2° N 3.9° W
Cothi	United Kingdom	Felin Mynachdy	300	234	3.44	51.9° N 4.2° W
Cree	United Kingdom	Newton Steward	367	243	3.90	55.0° N 4.5° W
Dart	United Kingdom	Austins Bridge	249	327	3.91	50.5° N 3.8° W
Dee	United Kingdom	Woodend	1394	512	2.46	57.1° N 2.6° W
Dove	United Kingdom	Rochester Weir	408	269	1.64	53.0° N 1.8° W
Frome (Bristol)	United Kingdom	Frenchay	191	70	1.01	51.5° N 2.5° W
Kinnel Water	United Kingdom	Redhall	78	245	3.45	55.2° N 3.4° W
Mole	United Kingdom	Gatwick Airport	35	88	0.81	51.1° N 0.2° W
Nith	United Kingdom	Friars Carse	812	293	3.28	55.1° N 3.7° W
South Tyne	United Kingdom	Haydon Bridge	763	348	2.19	55.0° N 2.2° W
Teifi	United Kingdom	Glan Teifi	898	211	2.81	52.0° N 4.6° W
Teme	United Kingdom	Tenbury	1164	229	1.13	52.3° N 2.6° W
Torridge	United Kingdom	Torrington	663	161	2.15	50.9° N 4.1° W
Tweed	United Kingdom	Boleside	1559	361	2.31	55.6° N 2.8° W
Wye	United Kingdom	Ddol Farm	167	387	3.76	52.3° N 3.5° W

HESSD
9, 12103–12143, 2012

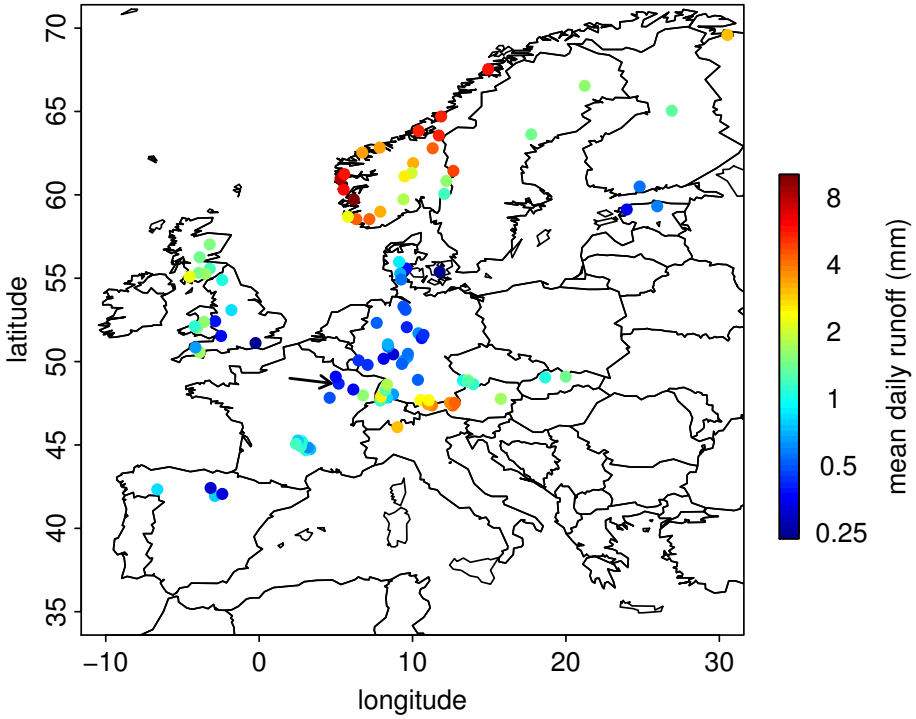

Fig. 1. Locations of the selected 106 catchments. The color coding indicates the mean daily runoff between May and September.

HESSD
9, 12103–12143, 2012

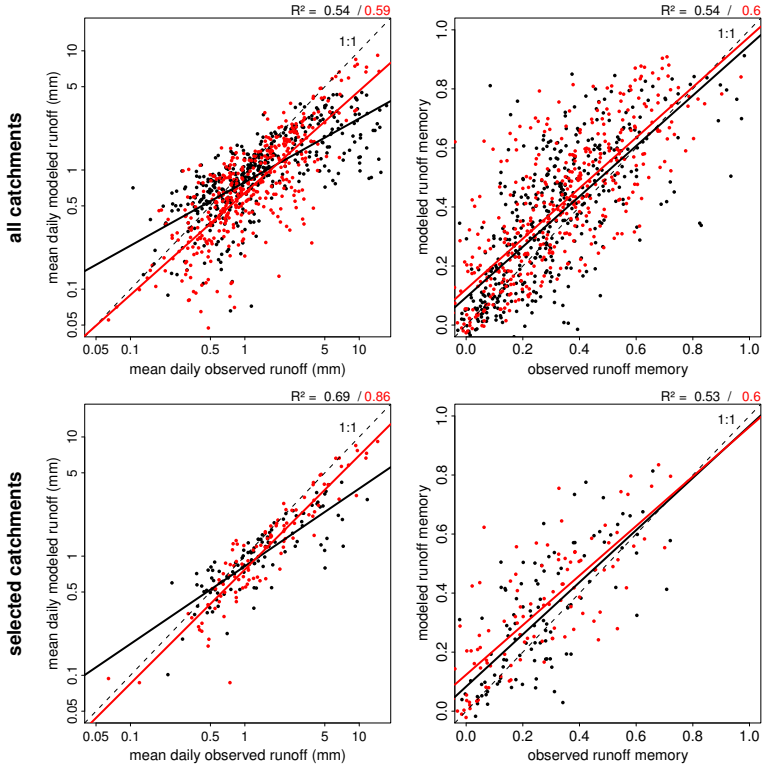

Fig. 2. The left plots show modeled versus observed mean daily runoffs for June (in black) and October (in red). Note the logarithmic scale of both axes. The thick straight lines are fitted with least-squared regression, R^2 values shown on top are a result of this. The right plots show the same, only for mean monthly runoff memory $\rho\left(Q_n, Q_{n+20\,\text{days}}\right)$. The upper row shows results for all 441 catchments, the lower row only contains the selected catchments.

HESSD
9, 12103–12143, 2012

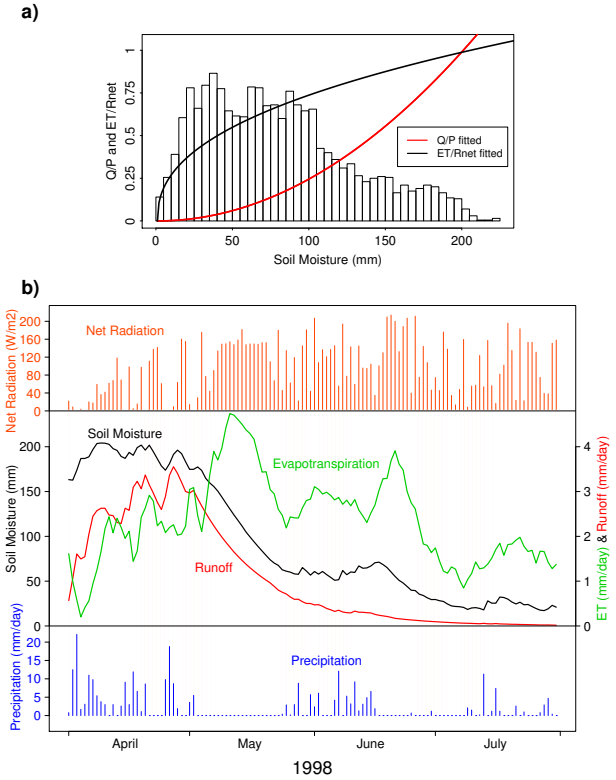

Fig. 3. (a) Fitted normalized runoff (Eq. 2) and ET (Eq. 3) functions for the Le Saulx catchment in Eastern France. The background histogram shows the relative abundance of soil moisture contents between April and October. **(b)** Time series of forcing (net radiation at the top, precipitation at the bottom) and according output of the simple model (soil moisture, runoff and ET in between the forcings) from the Le Saulx catchment during a pronounced dry-out period from April until July 1998.

HESSD
9, 12103–12143, 2012

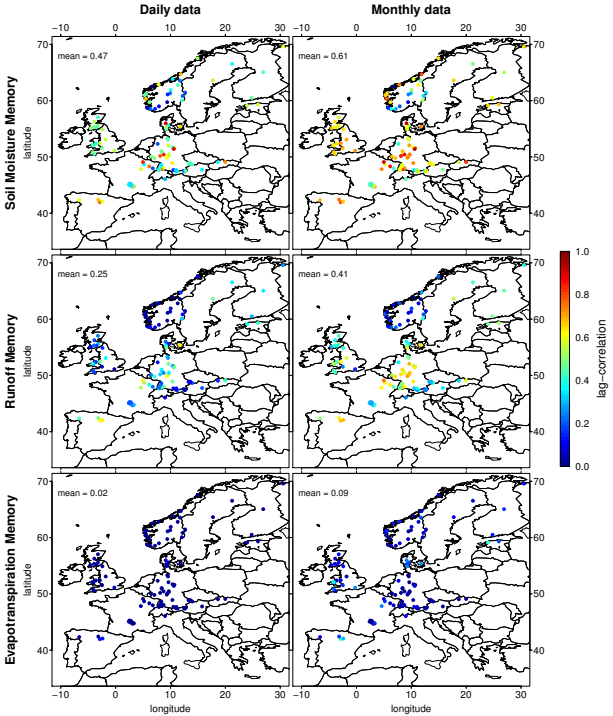

Fig. 4. Geographical distribution of mean May–September memories of soil moisture ($\rho\left(w_n, w_{n+\mathrm{lag}}\right)$, upper row), runoff ($\rho\left(Q_n, Q_{n+\mathrm{lag}}\right)$, center row) and ET ($\rho\left(E_n, E_{n+\mathrm{lag}}\right)$, lower row) for daily and monthly averaged data (all memories computed for a lag of 30 days (daily data) or 1 month (monthly data)) computed as described in Sect. 2.3.

HESSD
9, 12103–12143, 2012

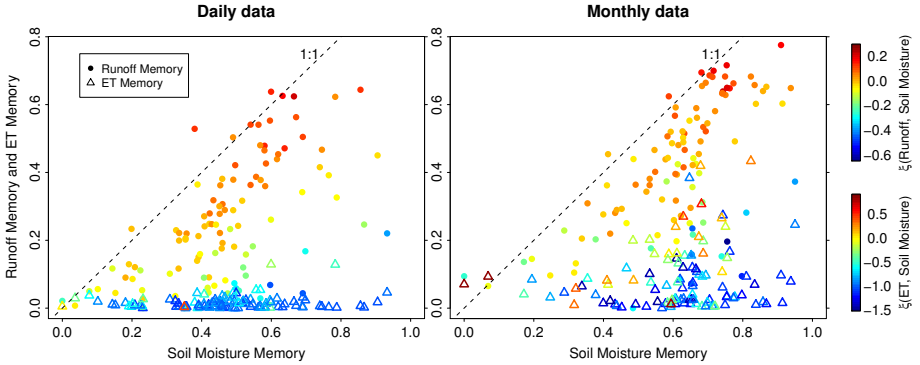

Fig. 5. Runoff (dots) and ET (triangles) memories $\rho\left(Q_n, Q_{n+\mathrm{lag}}\right)$ and $\rho\left(E_n, E_{n+\mathrm{lag}}\right)$, respectively, of all catchments plotted versus the corresponding soil moisture memories $\rho\left(w_n, w_{n+\mathrm{lag}}\right)$ for daily and monthly averaged data (all memories computed for a lag of 30 days (daily data) or 1 month (monthly data)). The color coding denotes the strength of the soil moisture-runoff coupling $\xi\left(Q_n, w_n\right)$ and the soil moisture-ET coupling $\xi\left(E_n, w_n\right)$, respectively (see Sect. 2.2).

HESSD
9, 12103–12143, 2012

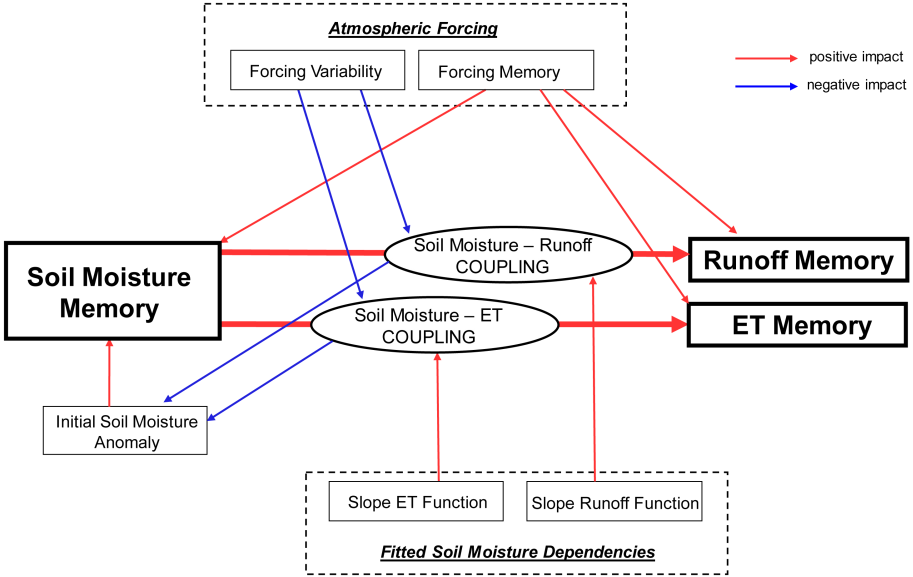

Fig. 6. Schematic view of propagation of soil moisture memory to runoff memory and ET memory. Red arrows denote positive impacts, blue arrows show negative impacts. Only dependencies investigated in this study are shown.

HESSD
9, 12103–12143, 2012

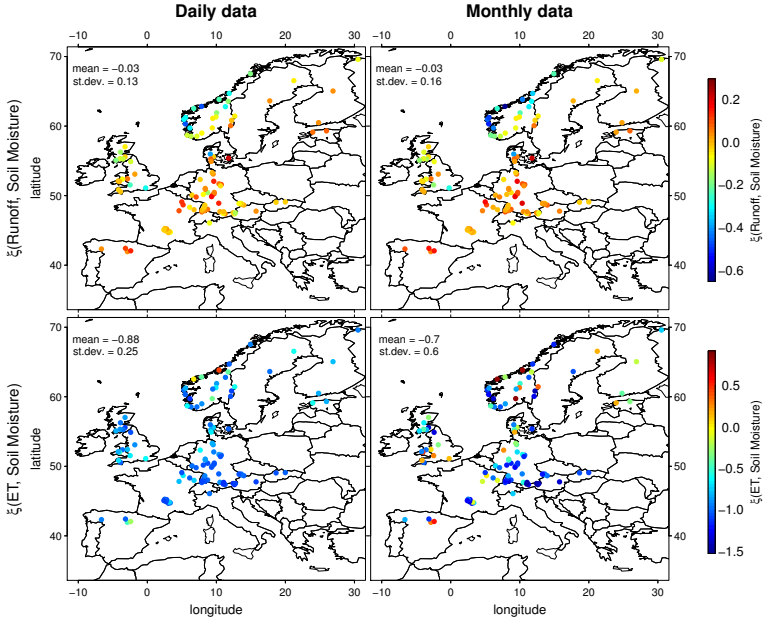

Fig. 7. Geographical distribution of mean May–September soil moisture-runoff (upper row) and soil moisture-ET (lower row) coupling strengths $\xi(Q_n, w_n)$ and $\xi(E_n, w_n)$, respectively, for daily and monthly averaged data. Respective strengths are shown through the color coding. In the upper left corner of each plot the mean and standard deviation over all catchments are displayed.

HESSD
9, 12103–12143, 2012

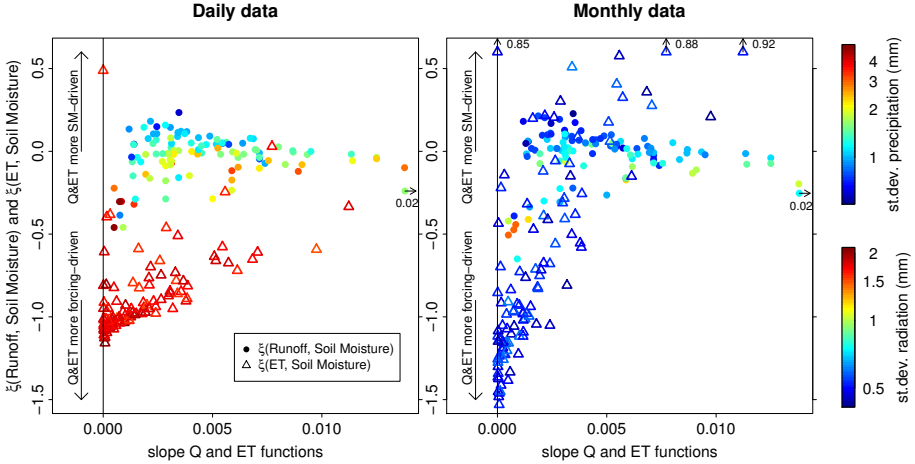

Fig. 8. Soil moisture-runoff (dots) and soil moisture-ET (triangles) coupling strengths, $\xi(Q_n, w_n)$ and $\xi(E_n, w_n)$, respectively, plotted against the respective runoff and ET function slope (computed as described in Sect. 4.4.2) for daily and monthly averaged data. The color coding denotes the variance of the weighted precipitation sum precipitation (P_n^*) and of radiation, respectively. All involved quantities computed as means from May–September. Points that do not fit with the range of the x- and/or y-axis are also included together with an arrow pointing in the direction of their actual location and the true value displayed next to it.

HESSD
9, 12103–12143, 2012

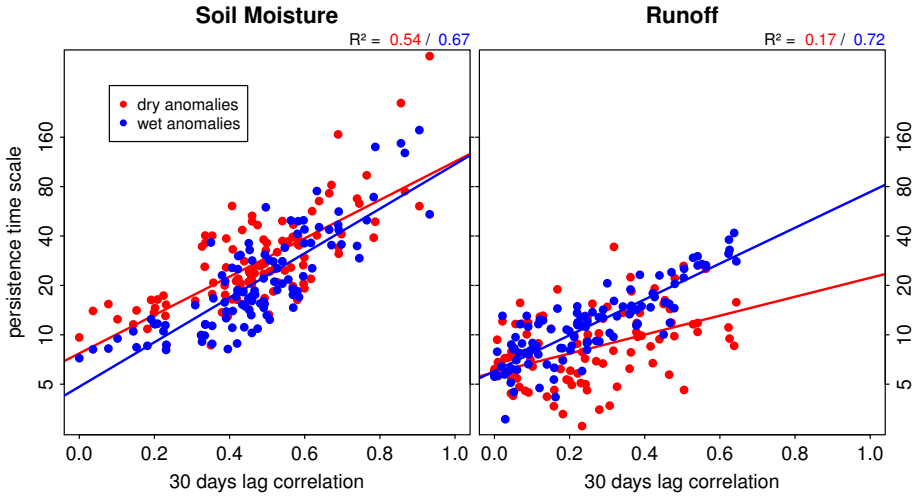

Fig. 9. Comparison of memory estimates computes as lag correlation and as persistence time scale (based on anomalies of 1.33 standard deviations from the mean) for soil moisture and runoff. Red points refer to persistence time scales estimated from dry anomalies whereas blue points are derived from wet anomalies. The red and blue lines denote the respective linear least-squares fit. Note the logarithmic scale of the persistence time scale.

HESSD
9, 12103–12143, 2012

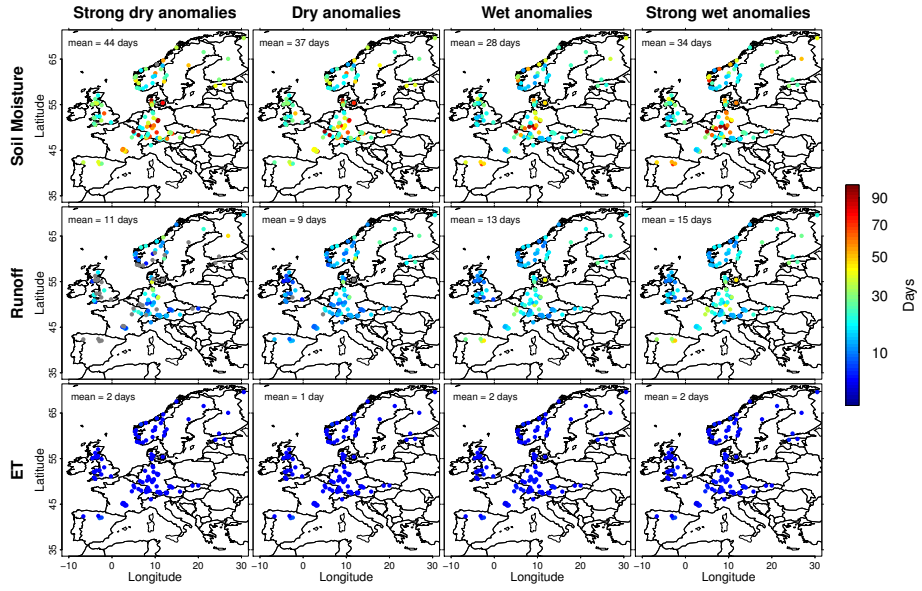

Fig. 10. Overview of mean durations to recover from (very) dry/wet conditions (1.33 and 1.66 standard deviations away from the respective daily mean of the respective quantity) to normal conditions (±1 standard deviation around the mean) for soil moisture, runoff and ET. The results are based on daily data. In the upper left corner of each plot the mean over all catchments is displayed.

HESSD
9, 12103–12143, 2012